Sulfate aerosol properties derived from combining coincident ACE-FTS and SAGE III/ISS measurements

C.D. Boone [a],[*], P.F. Bernath [a],[b], A. Pastorek [b], M. Lecours [a]

[a] *Department of Chemistry, University of Waterloo, 200 University Avenue West, Ontario N2L 3G1, Canada.*
[b] *Department of Chemistry and Biochemistry, Old Dominion University, Norfolk, VA 23529, United States of America*

ARTICLE INFO

ABSTRACT

Combining infrared aerosol transmittance spectra from the Atmospheric Chemistry Experiment Fourier transform spectrometer (ACE-FTS) and visible/near infrared extinction information from coincident SAGE III/ISS measurements, the properties of stratospheric sulfate aerosols are derived under various conditions. Assuming a bimodal size log-normal distribution (rather than a monomodal one) is required to properly characterize the spectra. Analysis is performed for enhanced sulfate conditions following two recent volcanic eruptions, the Raikoke eruption in 2019 and the Hunga Tonga-Hunga Ha'apai eruption in 2022, as well as for measurements under background sulfate conditions. The traditional analysis approach of assuming a monomodal distribution likely contributes to the large uncertainties for the impact of sulfate aerosols on climate.

1. Introduction

Stratospheric sulfate aerosols play an important role in climate [1] and in the chemistry [2] of the Earth's atmosphere. Particle size is a significant factor for both. For climate, sulfate aerosol size controls the balance between the cooling effect of scattering incoming radiation and the surface warming effect of absorbing both incoming and outgoing radiation [3]. For chemistry, the surface area available on the H_2O/H_2SO_4 droplet governs its effectiveness at facilitating heterogeneous reactions [1]. Sulfate aerosols are essential components of climate models, but quantifying their contribution to climate has long been a challenge, with large associated error bars [1,4]. Improved climate predictions depend on furthering our knowledge of aerosol physical and chemical parameters [5]. This will also help assess the potential utility (and dangers) of seeding sulfate aerosols for climate geoengineering [3].

Atmospheric infrared aerosol spectra are generated as a research product from the Atmospheric Chemistry Experiment (ACE), a satellite-based mission for remote sensing of the Earth's atmosphere that has been collecting measurements since February 2004 [6]. The mission employs the solar occultation measurement technique, collecting a series of measurements through the Earth's atmosphere as the Sun rises or sets from the orbiting satellite's perspective, providing up to 30 measurement opportunities per day. The primary instrument on board is the Atmospheric Chemistry Experiment Fourier Transform Spectrometer

(ACE-FTS), featuring high resolution (0.02 cm^{-1}, unapodized), broad spectral coverage (750 to 4400 cm^{-1}), and a signal-to-noise ratio ranging from ~100:1 up to ~400:1 [7]. There is also a pair of filtered imagers on board, providing atmospheric extinction profiles at 527.11 and 1020.55 nm [6]. The 527.11 nm imager data product suffers problems at low altitudes (below ~15 km) [8] and is not used in the current study, but the 1020.55 nm imager from ACE remains available for quantitative analysis.

Another Earth-observing mission providing information on aerosols is the Stratospheric Aerosol and Gas Experiment III instrument on the International Space Station (SAGE III/ISS), in operation since February 2017 [9]. It employs solar and lunar occultation, but only the solar occultation events will have close coincidences with ACE occultation events. SAGE III/ISS provides altitude profiles of aerosol extinction at nine wavelengths: 384.2, 448.5, 520.5, 601.6, 676.0, 756.0, 869.2, 1021.2, and 1543.9 nm.

Since the start of the SAGE III/ISS data record in 2017, two major volcanic eruptions have caused widespread, long-lasting perturbations of atmospheric sulfate aerosol levels. The first such eruption was on June 21, 2019, from the Raikoke volcano (latitude 48.3°N, longitude 153.3°E) on the Kuril Islands in the western Pacific Ocean. It injected a plume directly into the stratosphere, reaching altitudes of at least 14 km and rising more than 6 km over a span of 4 days following the eruption [10]. Material from the eruption settled into a persistent aerosol blanket

covering the latitude region north of ~45°N [11]. Aerosol optical depth at high northern latitudes remained elevated for up to a year following the eruption [12]. The second major eruption occurred January 15, 2022, from the Hunga Tonga-Hunga Ha'apai volcano (hereafter just Tonga), an underwater volcano in the South Pacific (latitude 20.5°S, longitude 175.4°W). The eruption was violent, with an energy release comparable to the largest atmospheric nuclear test explosion [13], creating a plume that reached altitudes as high as 57 km [14]. SO_2 in the plume rapidly converted to sulfate aerosols as a consequence of the high levels of ocean water carried into the stratosphere from the eruption [15]. By November 2022, sulfate aerosols from the Tonga eruption had spread around the world, with a particularly strong enhancement in the Southern Hemisphere [16]. At the time of this writing, more than 17 months after the eruption, sulfate aerosol levels remain strongly enhanced in the Southern Hemisphere stratosphere.

2. Methods

The ACE-FTS instrument features broad spectral coverage of the infrared region, while SAGE III/ISS provides data at shorter wavelengths. Infrared absorption (measured by the ACE-FTS) yields information on composition [11], while scattering in the near-infrared and visible regions deduced from SAGE III/ISS measurements provides insight into particle size. Combining the complementary information from the two instruments produces a fuller accounting of sulfate aerosol physical characteristics, including the percentage of H_2SO_4 in the droplet, the median radius, and the size distribution [17]. Both instruments employ solar occultation, providing data similar in character, but with different viewing geometries and instrumental configurations. The challenge becomes how to combine the two data sets in a robust, internally consistent manner in order to permit simultaneous analysis.

To that end, ACE-FTS and SAGE III/ISS data are spliced together into a combined aerosol transmittance spectrum. Data points from the ACE-FTS are generated as described in Boone et al. 2022 [11]. "Residual spectra" are derived through dividing ACE-FTS measurements by a calculated gas-phase spectrum based on ACE-FTS v4.1/4.2 retrieval results [18] using spectroscopic constants from HITRAN 2016 [19], as well as collision induced absorption contributions from N_2 [20] and O_2 [21], plus far wing contributions from the CO_2 ν_3 band [22]. The residual spectral are averaged into 2 cm^{-1} wide bins (slightly coarser than the 1.5 cm^{-1} spacing in the spectroscopic data employed in the analysis [23]), typically providing more than 1000 data points in the infrared aerosol spectrum. Systematic features in residual spectra are removed by calibrating with ACE-FTS "background measurements" that are closely matched to the target measurement's latitude, altitude, temperature, and time of year to ensure similar characteristics for the systematic features. More details on the methodology for this calibration are provided in Boone et al. 2022 [11]. Wavenumber regions involving HNO_3 bands missing from HITRAN 2016 [19] are excluded from the analysis in this study, to avoid the need to match HNO_3 contributions in the target and calibration measurements. Background sulfate aerosol contributions to the calibration measurements are estimated and removed (divided out) prior to performing the calibration [16], permitting the analysis of sulfate aerosols at background levels and avoiding the introduction of systematic errors into the intensities of measurements involving volcanically enhanced sulfate aerosols.

SAGE III/ISS provides altitude profiles for aerosol extinction at nine wavelengths. At each SAGE wavelength, the extinction profile can be used to calculate the equivalent transmittance for the tangent height (the altitude of closest approach to the surface for the measured solar ray) of a given ACE-FTS measurement. Ray tracing is used in a 'forward model' calculation to track the path a solar ray travels through the atmosphere for the known tangent height (previously derived by the ACE-FTS v4.1/4.2 retrievals) and atmospheric density profile (from the SAGE results). The solar ray follows a curved path as a result of atmospheric refraction. To account for refraction, the forward model calculations

employed here assume a wavelength in the infrared region (2400 cm^{-1}) rather than the given SAGE wavelength because the quantity of interest is the amount of absorption that would have occurred if light at that wavelength had followed the same path through the atmosphere as the infrared light measured by the ACE-FTS. The calculations average results over the ACE-FTS field of view, a 1.25 mrad circular aperture [8]. This approach offers the best possible internal consistency with the calibrated ACE-FTS residual spectra.

Rather than using provided uncertainties on SAGE extinction profiles to derive errors for the calculated transmittances, each SAGE data point is assigned a constant uncertainty of 0.002 in the nonlinear least squares fitting, overweighting these data points compared to those from the ACE-FTS, which are assigned a constant uncertainty of 0.02. This ensures that the SAGE data drives the determination of size parameters.

Data from the 384.2 nm SAGE channel was observed to be the most prone to large unphysical oscillations and was saturated at the tangent heights of several of the measurements analyzed in the current study (i. e., the extinction profile truncated at a relatively high altitude). It also often yields transmittances that appear to be inconsistent with the other channels, providing a slight 'hook' in the spectrum that severely impacts the results, particularly under background conditions, likely related to a previously reported potential bias in the channel from large molecular scattering [24]. Therefore, data from this SAGE channel are excluded from the analysis.

Note the implicit assumption is made that sulfates are the only aerosol type contributing to the signal, which could introduce systematic errors, particularly under background sulfate conditions where extinction levels are relatively low. Contributions from other aerosol types (as well as the spectral signature from nucleation particles in the droplet) in ACE-FTS spectra will cancel if the signal appears in both the target and calibration measurements, but no such calibration is applied to the SAGE data. The SAGE extinction signal, arising from scattering with a negligible absorption component, should not be overly sensitive to nucleation particles within the droplet but will be impacted by non-sulfate aerosols or cloud particles along its line-of-sight. However, the presence of non-sulfate particles in significant quantities would introduce spectral features in the ACE-FTS infrared spectrum, features that could not be reproduced in the analysis using sulfate aerosol optical constants. A lack of such features in the ACE-FTS spectrum serves as confirmation that the aerosols measured by SAGE are predominately sulfate.

The approach for calculating a sulfate aerosol infrared spectrum was previously described in detail [11]. Briefly, using optical constants from Lund-Myhre et al. [23], provided at a variety of wt% H_2SO_4 (the percentage of H_2SO_4 by weight in the solution) and temperature combinations relevant to atmospheric conditions, sulfate aerosol extinction coefficients as a function of wavenumber were calculated using IDL programs made available by the Earth Observation Data Group from the University of Oxford's Department of Physics (http://eodg.atm.ox.ac.uk/MIE/index.html), accounting for both absorption and Mie scattering by the spherical droplets. As described in Boone et al. 2022 [11], the Lund-Myhre data were extrapolated to lower temperatures to more fully encompass the range of atmospheric conditions encountered in ACE-FTS measurements.

The University of Oxford software assumes a log-normal size distribution of the following form:

$$n(r) = \frac{N_o}{\sqrt{2\pi}} \frac{1}{\ln(S)} \frac{1}{r} \exp\left[-\frac{(\ln(r) - \ln(r_m))^2}{2\ln^2(S)} \right], \tag{1}$$

where r is radius, r_m is median radius, N_o is particle density, and S is the distribution spread (typically referred to as the geometric width), which represents the distribution width (standard deviation) in ln(r) space.

Extinction coefficients calculated with the University of Oxford software were tabulated at median radii of 0.02, 0.05, 0.1, 0.2, 0.3, 0.4, 0.5, 0.6, 0.7, and 0.8 μm, with values for the distribution spread, S, of

1.05, 1.1, 1.2, 1.3, 1.4, 1.5, 1.6, 1.7, and 2.0 for each median radius. Calculating a sulfate aerosol spectrum (for use in least squares fitting) involves interpolating the tabulated data in S, $\ln(r_m)$, temperature, and wt% H_2SO_4, using cubic splines for the first two parameters followed by bilinear interpolation for the latter two parameters [11]. The Lund-Myhre optical constants span 400 to 7500 cm^{-1}, covering the full wavenumber range of the ACE-FTS instrument.

Optical constants used for the analysis of the SAGE III/ISS atmospheric extinctions are based on the data of Palmer and Williams [25]. Palmer and Williams report optical constants at 300 K for six compositions (25, 38, 50, 75, 84.5 and 95.6 wt% H_2SO_4) from 4000 to 27,800 cm^{-1}. In this wavenumber range, the imaginary component of the complex refractive index (absorption) is essentially zero and makes negligible contribution to the extinction coefficient. The real part (refractive index), however, is a function of temperature, T, and composition. The temperature variation of the refractive index can be calculated as outlined by Steele and Hamill [26], starting from the Lorentz-Lorenz equation. The refractive index, n(T), is given in Eq. (6) of Steele and Hamill [26] as a function of density, $\rho(T)$, at a given wavenumber and composition, w. The density was obtained from the polynomial expansion of $\rho(w,T)$ provided in Table 3 of Lund-Myhre et al. [23]. Using the University of Oxford software, the refractive index was calculated for the six Palmer and Williams compositions for the nine SAGE III/ISS wavenumbers as a function of temperature from 195 to 295 K in steps of 5 K. Calculations were performed for the same set of median radii and distribution spreads as was used for the tabulated Lund-Myhre data.

Using different sources of optical constants for the analysis of the two instruments could be a cause for concern if they are not internally consistent. The two sets of optical constants overlap, with both providing information for the SAGE point at 6477 cm^{-1} (1543.9 nm). Analysis of SAGE data employs optical constants from Palmer and Williams, but calculated transmittance at 6477 cm^{-1} using Lund-Myhre optical constants matches typically better than ~1.5 %. While this level of agreement is good enough to permit the combined analysis, it could introduce a systematic error, particularly for temperatures far from 300 K (the temperature at which the Palmer and Williams data were provided). There is insufficient information to estimate the impact on the analysis results presented here of using different sources of optical constants for the two instruments.

The tabulated data were calculated with an assumed density (N_o) of 40 particles/cm^3. Fitting of aerosol spectra assumes the usual Beer-Lambert expression for transmittance τ:

$$\tau = A * \exp\left[-\alpha L_{eff}\right], \qquad (2)$$

where L_{eff} is the effective path length, α is the extinction coefficient (the information calculated by the University of Oxford software), and A is an arbitrary baseline scaling factor. Note that A is assumed to be exactly 1.0 for SAGE data points in the analysis. The fitted value for A from ACE-FTS data is typically very close to 1.0. It is not possible to unambiguously derive particle density, N_o, from satellite limb measurements because the path length through the aerosol plume is unknown. From the measurement geometry, the path of sunlight travelling through the atmosphere is known, but the aerosol plume is not uniformly distributed along that path. There will be an altitude gradient and a horizontal gradient in particle density, both of which will contribute to gradients along the line of sight for the ACE-FTS measurement. Some portions of the path travelled by the measured sunlight will have aerosols at background levels. The quantity that can be determined from a limb measurement is column density, N_oL, the average particle density along the line-of-sight times the path length. In the current study, N_oL is equal to $40*L_{eff}$ (the assumed particle density of 40 particles/cm^3 in the tabulated data times the fitted value for the effective path length).

Sulfate aerosols have a propensity for forming a bimodal log-normal distribution, in both enhanced situations following volcanic eruptions

[27] and under background conditions [28]. The expression in Eq. (2) is appropriate for a monomodal size distribution. Applying a bimodal distribution to the analysis would lead to the following form:

$$\tau = A * \exp\left[-(\alpha_1 L_1 + \alpha_2 L_2)\right], \qquad (3)$$

where α_1 and L_1 refer to the extinction coefficient and effective path length, respectively, for one of the modes, while α_2 and L_2 refer to the quantities for the other mode. Each extinction coefficient (α_1 and α_2) will have its own values for r_m and S. A common value of wt% H_2SO_4 is assumed for both modes because it depends primarily on local conditions of temperature and H_2O vapor pressure [15,26]. The column density (N_oL) for mode 1 is calculated as $40*L_1$, while column density for mode 2 is $40*L_2$. The mode with smaller median radius is referred to as the "fine" mode, and the mode with larger median radius is referred to as the "coarse" mode.

The dependence of sulfate aerosol composition and size on temperature and H_2O leads to altitude gradients on these quantities [11]. However, for convenience, altitude gradients are ignored in the analysis presented here, which is sufficiently accurate because the geometry of limb measurements strongly weights the measurement sensitivity to the altitude region near the tangent point. Each spliced ACE-FTS and SAGE III/ISS transmittance spectrum is therefore treated as a pseudo gas cell measurement, assuming single values for temperature and wt% H_2SO_4 rather than deriving altitude profiles for these quantities. Although temperature can be derived from the measurement, to reduce the number of adjusted parameters it is instead fixed to the ambient value determined in the v4.1/4.2 retrievals [18]. Changing the fixed value for temperature by its uncertainty yields differences in fitted parameters (wt % H_2SO_4, median radius, etc.) that are fractions of their random errors [11], which indicates this approach provides sufficient accuracy.

3. Observations

3.1. ACE and sage coincidences

Combining ACE-FTS and SAGE III/ISS measurements requires finding coincidences, instances where the two instruments were measuring very similar air masses. The coincidences chosen for this study are listed in Table 1. An effort was made to find coincidences for different lengths of time after both the Raikoke and Tonga eruptions, to evaluate possible evolution of volcanically sourced sulfate aerosols as they age. Overlap between measurements from the two instruments is generally better in the Northern Hemisphere, with several coincidences featuring time separations of a few minutes and locations within a degree in both longitude and latitude, as seen in Table 1. Coincidences are less tight for Tonga measurements in the Southern Hemisphere, but the long-term stability of the Tonga plume during August and October (for occultations ss102428 and ss103255, respectively) suggests a degree of homogeneity that should allow the ACE and SAGE measurements to be reliably combined despite a larger geographic separation.

The 1 μm (1020.55 nm) imager from ACE provides a means to verify that the two instruments are measuring comparable scenes, by ensuring that its aerosol extinction profile agrees well with that from the 1 μm (1021.2 nm) SAGE channel. A number of potential ACE/SAGE matches were discarded because a cloud impacted one of the measurements but not the other. Fig. 1 shows the comparisons of 1 μm aerosol extinction for selected ACE/SAGE coincidences. The SAGE data sometimes shows (likely unphysical) oscillations, but the impact of these oscillations on the analysis is implicitly reduced by averaging the transmission calculation over the ACE-FTS field of view.

3.2. Raikoke

As indicated in Table 1, three mid-latitude coincidences between ACE and SAGE III/ISS were selected for the period following the Raikoke

Table 1

Coincident solar occultation events for ACE and SAGE III/ISS. Latitude is for the ACE event. The name of the SAGE event indicates the date (year, month, day, and event number: yyyymmdd##). Separations in time, latitude, and longitude are absolute values of the differences for the two events.

| ACE event	SAGE III/ISS event	Latitude (°)	Δ time (minutes)	Δ latitude (°)	Δlongitude (°)	Type
ss84200	2019033036	58.7	1.7	0.9	0.2	Background
ss84219	2019040103	55.7	2.3	0.9	0.3	Background
sr86637	2019091137	58.0	2.0	0.2	0.4	Raikoke
sr88283	2020010112	46.9	5.5	3.0	1.5	Raikoke
ss89663	2020040334	45.5	3.3	0.7	0.7	Raikoke
sr99051	2021123021	43.7	0.7	0.1	0.3	Background
ss100628	2022041609	−28.7	1.1	0.6	0.1	Tonga
ss102428	2022081606	−26.4	17	3.4	3.2	Tonga
ss103255	2022101109	−15.0	16	4.3	3.4	Tonga
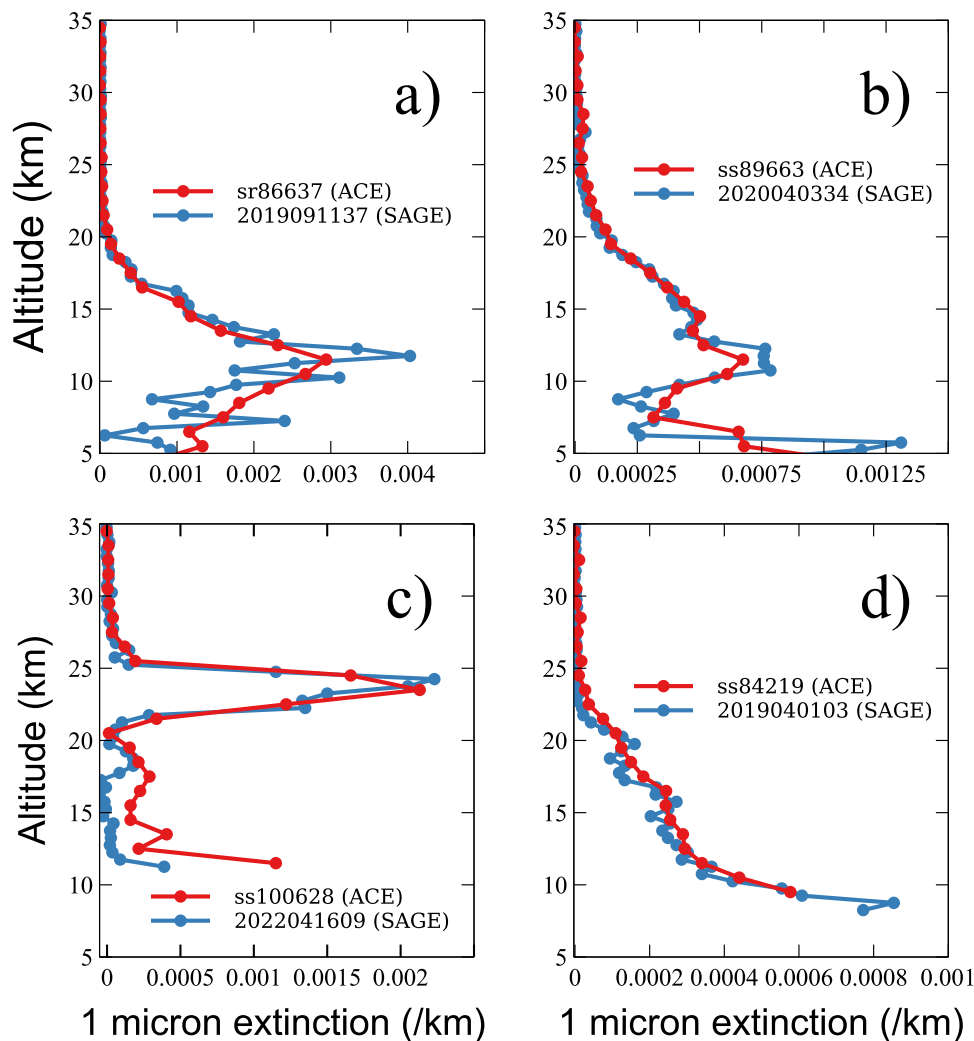
Fig. 1. 1 μm aerosol extinction for pairs of coincident ACE and SAGE III/ISS measurements. (a) sr86637 [September 11, 2019, latitude 58.0°N, longitude 157.4°E] and SAGE 2019091137, containing sulfates from the Raikoke eruption. (b) ss89663 [April 3, 2020, latitude 45.5°N, longitude 13.8°E] and SAGE 2020040334, also from the Raikoke eruption. (c) ss100628 [April 16, 2022, latitude 28.7°S, longitude 171.2°E] and SAGE 2022041609, containing sulfates from the Tonga eruption. (d) ss84219 [April 1, 2019, latitude 55.7°N, longitude 102.5°W] and SAGE 2019040103, with background-level sulfates. Note the different x-axis scales.

eruption. The first coincidence was in September 2019, three months after the eruption, the second was in January 2020, and the final coincidence in this study attributed to Raikoke was in April 2020. The intention was to search for sulfate evolution in aging aerosols but note that each coincidence falls in a different season (northern autumn, winter, and spring). Seasonal variations in temperature and H$_2$O are significant at the given latitudes, which will contribute to aerosol evolution but could obscure aging effects.

Fig. 2 shows analysis results for the measurement at 15.2 km in

sr86637. The results in Fig. 2a come from fitting the data to a monomodal distribution, using an expression of the form in Eq. (2), while the results in Fig. 2b come from fitting to the bimodal form in Eq. (3). The data points at lower wavenumber (i.e., in the infrared) in the plots are from the ACE-FTS. The eight data points at higher wavenumber are from SAGE III/ISS. In the least squares fitting, SAGE data points were overweighted so they would dominate the analysis rather than the 1200+ data points from the ACE-FTS.

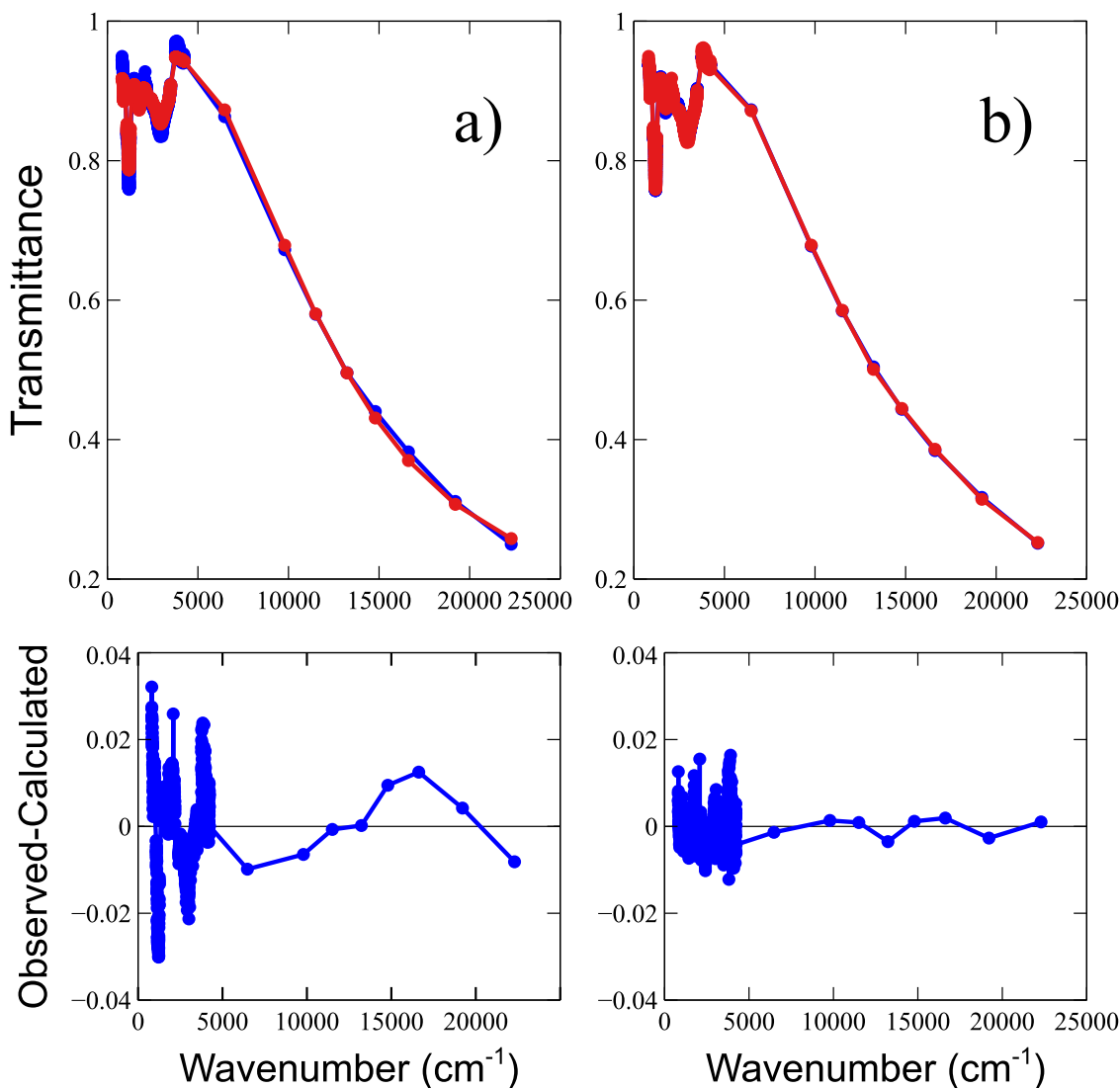As is evident in Fig. 2, assuming a monomodal distribution in the

Fig. 2. Combined ACE-FTS and SAGE III/ISS transmittance fitting results for the measurement at tangent height 15.2 km in ACE occultation sr86637. The coincident SAGE event is 2019091137. The top plots show the measurement in blue and the fitted result in red, while the bottom plot shows the residuals (observed – calculated). (a) Assuming a monomodal distribution. (b) Assuming a bimodal distribution.

analysis yields unsatisfactory results. There is a clear difficulty balancing the signal from absorption in the infrared and scattering in the short-wave region. With the overweighted SAGE data driving the least squares fitting, the monomodal results in Fig. 2a underestimate the amount of absorption in the infrared (ACE-FTS) region. The curvature of the SAGE transmittances is also reproduced with limited accuracy in Fig. 2a, making the SAGE residuals exhibit systematic behavior. Assuming a bimodal distribution reproduces the data much better, as shown in Fig. 2b. This pattern holds for all measurements analyzed with sulfate aerosols from the Raikoke eruption: a bimodal distribution yields far superior results than can be achieved when using a monomodal distribution.

When fitting to a bimodal distribution, the least squares fitting shows evidence of being slightly underconstrained. Convergence is slow, and the random fitting errors (i.e., the square root of the diagonal covariance matrix elements) are relatively large. For the measurement from Fig. 2b, the random fitting errors for r_m and S for the two modes were the order of 30–40 %. To achieve a more robust convergence and reduce fitting errors, S(fine) was fixed to 1.65, a rough average of the value determined for all the Raikoke measurements. With this implemented, the random fitting error for r_m(coarse) is reduced to about 20 %, while the random errors for r_m(fine) and S(coarse) reduce to less than 10 %. There

could be significant systematic error associated with r_m(fine) because the fitted value for median radius depends strongly on the assumed value of S for the given mode. However, the parameters determined for the coarse mode do not depend strongly on the assumed value for S (fine).

Unfortunately, every measurement associated with the Raikoke eruption has two viable solutions, two different results with nearly identical fitting quality (i.e., nearly identical minimum chi-squared value in the least squares analysis). The existence of two comparable chi-squared minima is presumably a consequence of the bimodal distribution being the product of two independent curves, providing a mathematical flexibility in determining the relative contributions from the fine and coarse modes when there is no distinctive structure in the SAGE portion of the spectrum (as is the case for the Raikoke measurements). We must therefore choose which is the more likely solution. Fig. 3 breaks down the contributions to the signal from the fine and coarse modes from the two possible solutions for the fitting results in Fig. 2b. The fitting results for each solution are provided in the caption to Fig. 3, including random fitting errors. The random fitting errors are better for the solution with smaller r_m and larger S for the coarse mode (0.28 μm and 1.40, respectively), and that solution is more in line with observations from the Atmospheric Tomography (ATom) mission [29],
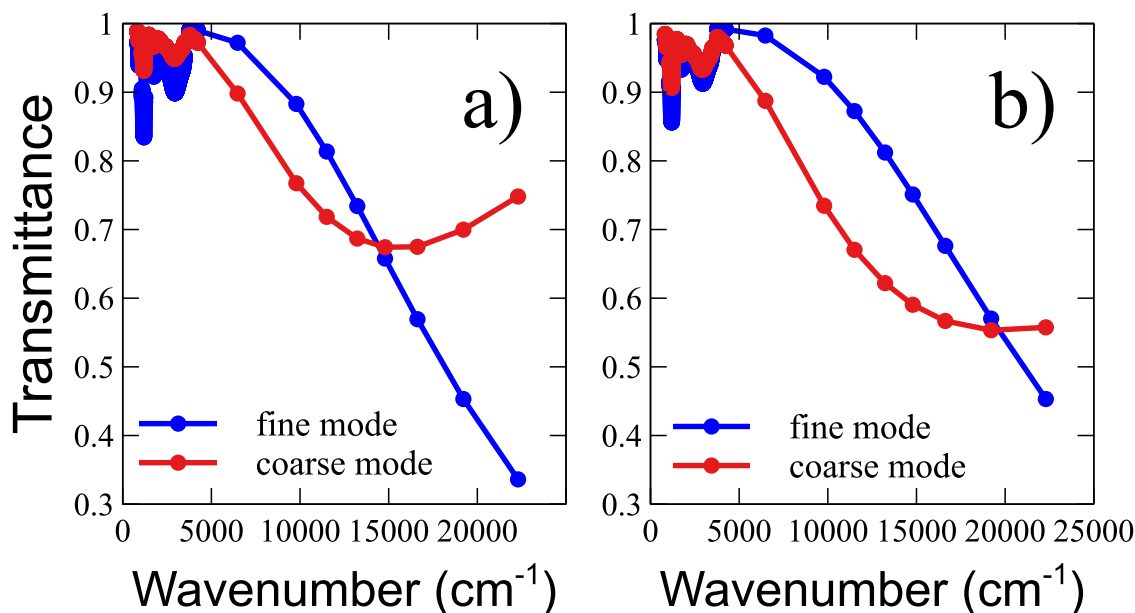
Fig. 3. Contributions to the calculated spectrum for the fitting result in Fig. 2b from the fine and coarse modes (in blue and red, respectively). The calculated spectrum is the product of the two curves. There are two solutions with nearly identical fitting quality. (a) r_m(fine) = 0.059 ± 0.003 μm, S(fine) = 1.65 (fixed), r_m(coarse) = 0.44 ± 0.10 μm, S(coarse) = 1.15 ± 0.18, and N_o(fine)/N_o(coarse) ≈ 380. (b) r_m(fine) = 0.053 ± 0.003 μm, S(fine) = 1.65 (fixed), r_m(coarse) = 0.28 ± 0.06 μm, S(coarse) = 1.40 ± 0.10, and N_o(fine)/N_o(coarse) ≈ 130. Reported uncertainties are random fitting errors and do not include systematic errors.

more of a consideration for the Raikoke occultations in 2020, where sulfate aerosols are trending toward background levels. Thus, the result depicted in Fig. 3b is selected as the preferred solution.

Table 2 shows fitting results for all analyzed measurements associated with the Raikoke eruption. These results correspond to the preferred solution, with smaller r_m and larger S for the coarse mode. Although it is not possible to measure particle density (N_o), the fitting results provide an estimate of the relative abundances of the fine and coarse modes, N_o(fine)/N_o(coarse), through the ratio of the column densities (N_oL) of the two modes with the assumption of a common path length. Because there is nothing in the spectra themselves that would exclude the alternative solution, featuring larger r_m and smaller S for the coarse mode, results for that solution are provided in Appendix A for reference.

3.3. Tonga

Three Southern Hemisphere tropical/subtropical ACE and SAGE III/ISS coincidences were observed from the time following the Tonga eruption. The first occurred in April 2022, roughly three months after the eruption, the second was from August 2022, and the third was from October 2022. See Table 1 for the details of the coincidences.

Fig. 4 shows the fitting results for one of the Tonga measurements (ss100628 at 23.6 km). Once again, a bimodal size distribution yields a significant improvement in fitting residuals compared to a monomodal distribution.

Fig. 5 shows the contributions to the calculated spectrum for the results in Fig. 4b. For Tonga, the coarse mode contribution to the spectrum is so pronounced relative to the fine mode that there is only one viable solution, unlike Raikoke. Parameters for the fine mode are significantly less well determined than for Raikoke. With no constraints applied in the analysis of Tonga measurements, fitting errors for S(fine)

Table 2

Fitted sulfate parameters using a monomodal and a bimodal distribution for measurements associated with the Raikoke eruption. Fine mode refers to the mode with the smaller median radius in the bimodal distribution, while coarse mode refers to the mode with the larger median radius. The abundance ratio, N_o(fine)/N_o(coarse), is calculated from the ratio of the fitted column densities (N_oL), assuming a common path length, L. Wt% H_2SO_4 is from the bimodal distribution fit.

ACE event	Altitude (km)	Mono r_m (μm)	Mono S	Fine r_m (μm)	Fine S	Coarse r_m (μm)	Coarse S	N_o(fine)/ N_o(coarse)	wt% H_2SO_4
sr86637	17.5	0.130	1.59	0.052	1.65*	0.23	1.55	130	73.8
	15.2	0.146	1.58	0.053	1.65*	0.28	1.40	130	73.1
	13.0	0.141	1.58	0.064	1.65*	0.23	1.49	40	71.2
	10.9	0.140	1.59	0.063	1.65*	0.16	1.63	10	67.0
sr88283	17.0	0.123	1.57	0.062	1.65*	0.37	1.23	300	70.0
	16.0	0.122	1.58	0.065	1.65*	0.31	1.33	120	70.0
	15.1	0.127	1.57	0.060	1.65*	0.28	1.35	100	69.7
	14.1	0.132	1.56	0.058	1.65*	0.27	1.37	90	69.6
	13.2	0.135	1.56	0.053	1.65*	0.26	1.37	100	68.3
	12.3	0.137	1.56	0.053	1.65*	0.25	1.40	86	67.8
	11.6	0.138	1.56	0.053	1.65*	0.25	1.40	88	66.6
	10.8	0.165	1.50	0.061	1.65*	0.27	1.39	71	65.6
ss89663	16.6	0.126	1.53	0.059	1.65*	0.29	1.34	180	70.6
	14.5	0.125	1.55	0.057	1.65*	0.26	1.36	110	70.9
	12.6	0.126	1.56	0.061	1.65*	0.23	1.42	61	70.0
	11.1	0.126	1.57	0.062	1.65*	0.27	1.38	95	66.8

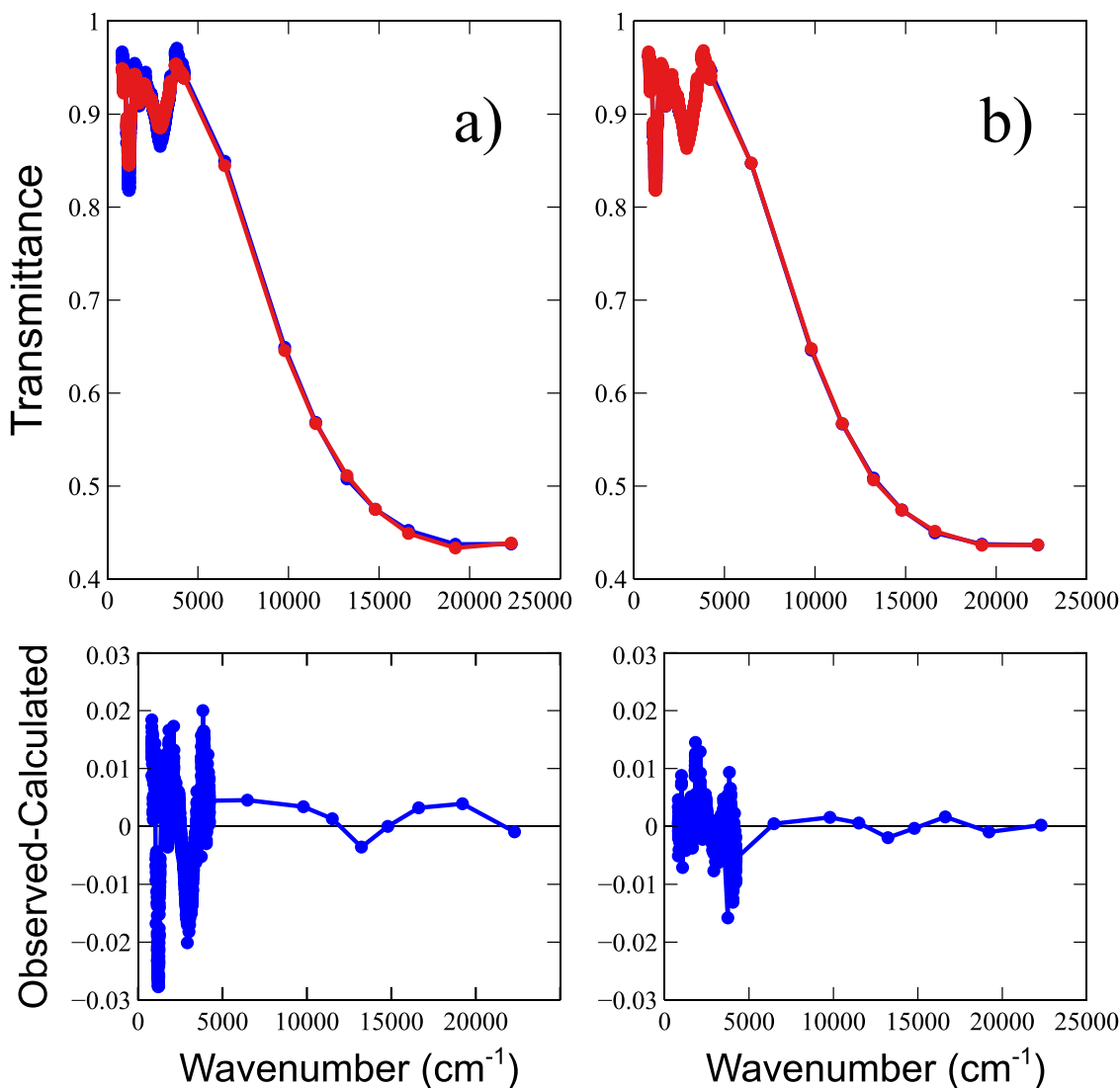* S fixed to the indicated value in the analysis.

Fig. 4. Combined ACE-FTS and SAGE III/ISS transmittance fitting results for the measurement at tangent height 23.6 km in ACE occultation ss100628. The coincident SAGE event is 2022041609. The top plots show the measurement in blue and the fitted result in red, while the bottom plot shows the residuals (observed – calculated). (a) Assuming a monomodal distribution. (b) Assuming a bimodal distribution.
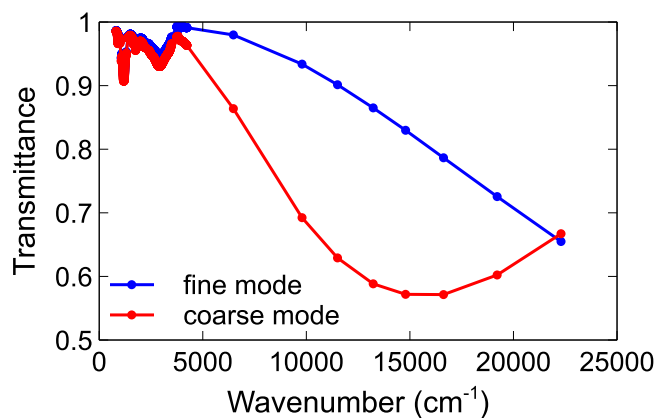

Fig. 5. Contributions to the calculated spectrum for the fitting result in Fig. 4b from the fine and coarse modes (in blue and red, respectively). The calculated spectrum is the product of the two curves. r_m(fine) = 0.050 ± 0.003 μm, S(fine) = 1.65 (fixed), r_m(coarse) = 0.44 ± 0.02 μm, S(coarse) = 1.12 ± 0.05, and N_o(fine)/N_o(coarse) ≈ 190. Reported uncertainties are random fitting errors and do not include systematic errors.

are greater than 60 %, and errors on r_m(fine) are greater than 100 %, indicating insufficient information content to determine both parameters for the fine mode. These fitting errors (along with the variability in fitted values from measurement to measurement) are perhaps too large to be considered reliable for generating a rough average for S(fine), and so for the analysis of Tonga measurements the parameter is fixed to the same value used for Raikoke: 1.65. This provides fitting errors for r_m(fine), r_m(coarse), and S(coarse) that are better than 5, 6 %, as seen for the errors shown in the caption to Fig. 5. Again, there could be a significant systematic error in r_m(fine), but neither the values nor the fitting errors for the coarse mode parameters change significantly for different choices of S(fine). Fitting results for Tonga measurements are provided in Table 3.

3.4. Background aerosol case

Three extremely close coincidences between ACE and SAGE at northern midlatitudes featuring sulfate aerosols at background levels were selected for analysis. See Table 1 for the specifics of the occultations. All three coincidences had very good agreement for the 1 μm aerosol extinction profiles from ACE and SAGE (see, e.g., Fig. 1d). Fig. 6 shows an example fitting result (ss84200 13.3 km) for sulfate aerosols at

Table 3

The same as Table 2, but for measurements associated with the Tonga eruption.

ACE event	Altitude (km)	Mono r_m (μm)	Mono S	Fine r_m (μm)	Fine S	Coarse r_m (μm)	Coarse S	N_o(fine)/ N_o(coarse)	wt% H_2SO_4
ss100628	24.8	0.225	1.51	0.043	1.65*	0.44	1.12	510	74.3
	23.6	0.281	1.40	0.050	1.65*	0.44	1.12	190	74.1
	22.4	0.283	1.39	0.092	1.65*	0.44	1.15	25	73.3
ss102428	23.2	0.192	1.42	0.044	1.65*	0.38	1.12	620	72.2
	21.8	0.195	1.53	0.047	1.65*	0.40	1.11	240	70.2
	20.5	0.269	1.39	0.062	1.65*	0.43	1.11	70	69.8
	19.3	0.270	1.40	0.074	1.65*	0.45	1.11	48	68.4
	18.0	0.232	1.48	0.094	1.65*	0.46	1.12	41	69.0
ss103255	23.6	0.165	1.55	0.051	1.65*	0.36	1.17	150	73.0
	21.5	0.258	1.40	0.063	1.65*	0.42	1.11	64	70.1
	19.6	0.249	1.45	0.090	1.65*	0.39	1.22	16	69.1

* S fixed to the indicated value in the analysis.
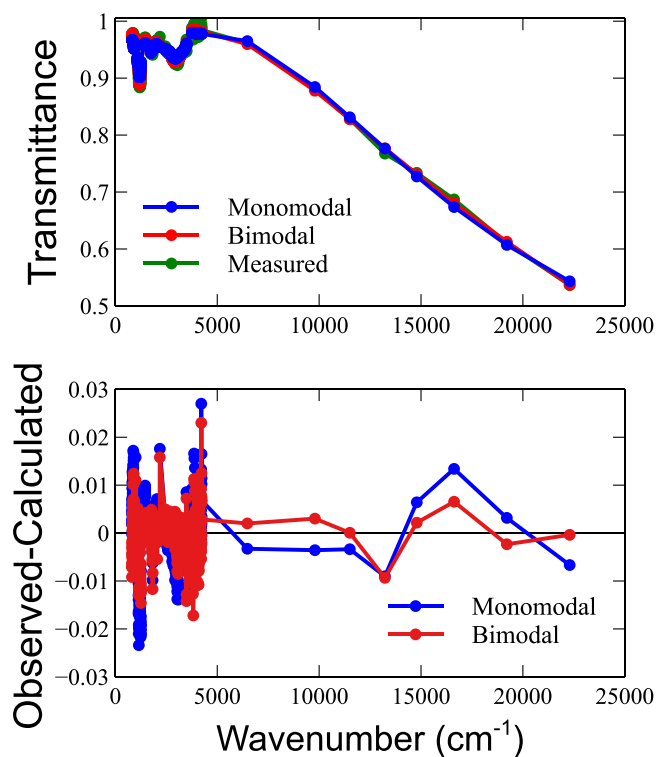

Fig. 6. Combined ACE-FTS and SAGE III/ISS transmittance fitting results for the background measurement at tangent height 13.3 km in ACE occultation ss84200. The coincident SAGE event is 2019033036. The top plot shows the measurement in green, the bimodal fitted result in red, and the monomodal fitting result in blue. The bottom plot shows the fitting residuals (observed – calculated), with the bimodal results plotted in red and the monomodal results in blue.

background levels. Although the effect is less dramatic than the volcanic cases, absorption in the infrared in Fig. 6 is clearly underestimated when assuming a monomodal distribution, and there is a noticeable improvement in the fitting residuals when using a bimodal distribution.

Note that there is systematic behavior in SAGE residuals when using a bimodal distribution, particularly evident in Fig. 6, that appears in the same basic form for all analyzed measurements (see Figs. 2b and 4b) but appears to be slightly more pronounced for the background cases. The source of this behavior is not currently known but could be at least partially spectroscopic in nature. Particularly evident is a persistent sharp dip in the residuals near 13,228 cm^{-1} (756.0 nm), which is in the vicinity of the O_2 A-band, suggesting the contribution from that spectral feature might not be completely removed in the aerosol extinction data product for SAGE III/ISS.

The contributions from the two modes for ss84200 13.3 km are

shown in Fig. 7. Both modes contribute significantly to the extinction, with the coarse mode providing larger scattering than the fine mode in the near-infrared region. Unfortunately, low signals from background sulfate aerosols are such that it becomes impossible to perform a reliable quantitative analysis for a bimodal size distribution. With S(fine) fixed to 1.65, the fitting errors on S(coarse) are the order of 40 %, while errors on r_m(coarse) are over 100 %. The primary cause of the large fitting errors appears to be the systematic residuals in the SAGE data seen in Fig. 6. Excluding the data point near 13,228 cm^{-1} from the analysis would yield significantly improved fitting errors, but with no independent evidence of problems in this channel, removing it would be an arbitrary decision. Fuller investigation of the background sulfate aerosol case requires further assessment of the source(s) of systematic residuals in the SAGE III/ISS data.

For the bimodal analysis of background aerosols presented here (collected in Table 4), S(coarse) is fixed to 1.40, the representative value for S(coarse) observed by the ATom mission [29], and the value that Raikoke measurements trend towards as sulfate aerosols decline toward background levels (see Table 2). With both S(fine) and S(coarse) fixed, the bimodal fitting results are of limited use. Unlike the volcanic cases, where coarse mode results were relatively 'unpolluted' by fixing a quantity for the fine mode, fitted parameters for both modes will potentially have systematic errors. However, the fitting results will give a sense of the relative contributions of the two modes to the signal for the background case.
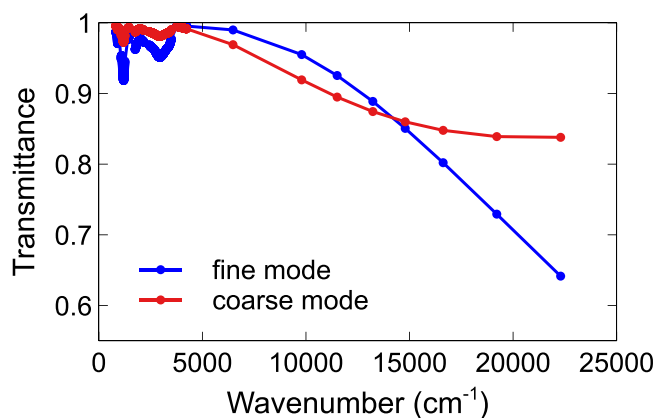

Fig. 7. Contributions to the calculated spectrum for the bimodal fitting result in Fig. 6 from the fine and coarse modes (in blue and red, respectively). The calculated spectrum is the product of the two curves. r_m(fine) = 0.053 ± 0.002 μm, S(fine) = 1.65 (fixed), r_m(coarse) = 0.27 ± 0.01 μm, S(coarse) = 1.40 (fixed), and N_o(fine)/N_o(coarse) ≈ 200. Reported uncertainties are random fitting errors and do not include systematic errors.

Table 4

The same as Table 2, but for measurements associated with background sulfate aerosols.

ACE event	Altitude (km)	Mono r_m (μm)	Mono S	Fine r_m (μm)	Fine S	Coarse r_m (μm)	Coarse S	N_o(fine)/ N_o(coarse)	wt% H_2SO_4
ss84200	15.5	0.118	1.56	0.056	1.65*	0.29	1.40*	260	73.9
	13.3	0.124	1.54	0.054	1.65*	0.27	1.40*	200	72.5
	11.5	0.124	1.54	0.053	1.65*	0.25	1.40*	160	69.2
ss84219	14.5	0.118	1.56	0.058	1.65*	0.28	1.40*	200	70.4
	12.6	0.124	1.55	0.053	1.65*	0.26	1.40*	170	69.7
	11.5	0.122	1.55	0.058	1.65*	0.26	1.40*	140	67.4
sr99051	16.2	0.110	1.56	0.064	1.65*	0.29	1.40*	220	72.4
	15.4	0.110	1.57	0.064	1.65*	0.27	1.40*	170	70.8
	14.7	0.107	1.58	0.067	1.65*	0.28	1.40*	170	71.5
	13.9	0.115	1.55	0.061	1.65*	0.24	1.40*	110	69.9
	13.1	0.112	1.56	0.064	1.65*	0.25	1.40*	110	71.4
	12.3	0.117	1.54	0.059	1.65*	0.24	1.40*	100	69.9
	11.7	0.111	1.57	0.067	1.65*	0.26	1.40*	130	69.9
	11.1	0.110	1.57	0.068	1.65*	0.28	1.40*	170	69.3

* S fixed to the indicated value in the analysis.

3.5. Summary

For comparison of results from different events, it is convenient to calculate the effective radius (r_{eff}) of the distribution, defined by the area-weighted mean radius [30]:

$$r_{eff} = \frac{\int r^3 n(r) dr}{\int r^2 n(r) dr},$$ (4)

where $n(r)$ is the lognormal distribution described in Eq. (1). This condenses the size distribution information into a single parameter that reduces potential variability from the strong anti-correlation between S and r_m. All size distribution information from Table 2 through 4 is plotted in Fig. 8.

Looking at Fig. 8, r_{eff} is significantly larger for the Tonga observations, particularly the profile that extends to the highest altitude, which relates to the occultation from April 2022 (ss100628), the 'youngest' Tonga measurement shown in the figure. Fine and coarse mode r_{eff} profiles are similar for Raikoke and background cases, but the monomodal effective radius for Raikoke is larger because coarse mode particles represent a higher proportion of sulfate aerosols for Raikoke than for the background case, as seen in Fig. 9: N_o(fine)/N_o(coarse) is smaller for the Raikoke results than for the background examples.

The Raikoke monomodal profile showing the highest r_{eff} in Fig. 8 is from sr86637, the youngest Raikoke aerosols observed in this study. The observed values of r_{eff} for this occultation (from September 11th, 2019) agree well with the August 2019 results reported in Wrana et al. 2023 [31], which were derived from SAGE III/ISS measurements. Looking at the three profiles in Fig. 8 from Raikoke for the monomodal distribution, r_{eff} trends steadily toward background values as the 'aerosol blanket' from Raikoke ages.
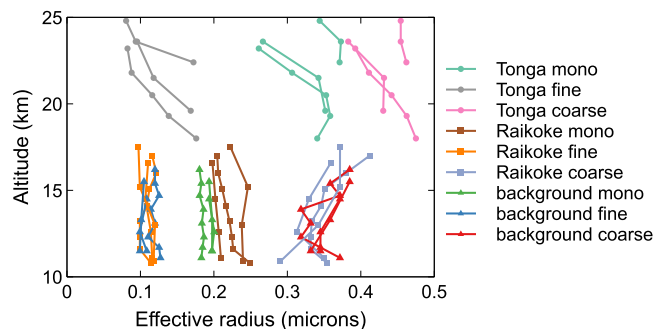

Fig. 8. Effective radius profiles for the example occultations, including monomodal and bimodal (fine and coarse mode) lognormal distributions. Results are calculated from the size distribution information in Table 2 through 4. Each curve is from a different occultation.
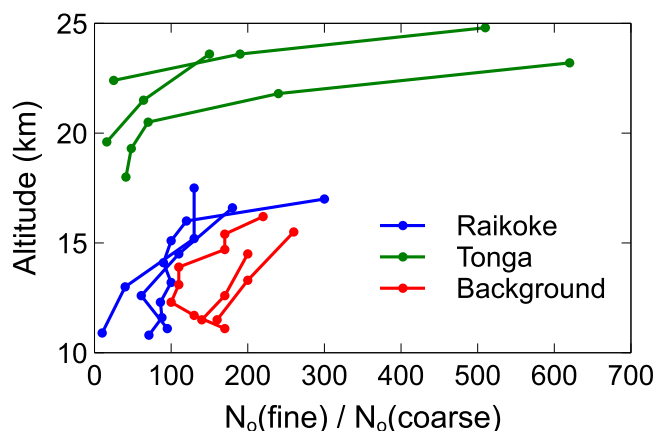

Fig. 9. The ratio of fine mode number density to that of the coarse mode, taken from the bimodal distribution results in Table 2 through 4.

A previous measurement of r_{eff} for Tonga sulfate aerosols from April 2022 reported a peak value around 0.4 μm, using SAGE III/ISS measurements and assuming 'background' sulfate composition [32]. As seen in Table 3, wt% H_2SO_4 for ss100628, the ACE-FTS occultation from April 2022, was between 73 and 75 %, close to the typical composition assumed for background aerosols of 75 %. The effective radius for ss100628 from Fig. 8 (the Tonga monomodal profile with the highest r_{eff}) peaks a bit below 0.4 μm, which represents fairly good agreement.

4. Discussion and conclusion

For both volcanic and lower-stratospheric background cases, combined ACE-FTS and SAGE III/ISS spectra are better reproduced by a bimodal size distribution than a monomodal distribution. Employing a monomodal distribution in the analysis when the true distribution is more accurately represented by a bimodal distribution exacerbates errors on values derived for aerosol size and number density [33]. Assuming a bimodal distribution would have an impact on the inferred role sulfate aerosols play in climate [34]. The standard approach in the literature of assuming a monomodal distribution likely accounts for a significant portion of the large uncertainties ascribed to sulfate aerosols' contributions to climate change [1,4]. Deriving monomodal sulfate aerosol information from shortwave measurements will underestimate absorption in the infrared (see, e.g., Fig. 2), thereby underestimating its 'greenhouse' effect on climate.

Instruments that measure scattered sunlight rather than extinction need to assume properties for the aerosols in order to analyze the data [35]. It has been shown from limb scattering measurements of Tonga

sulfate aerosols that assuming the wrong size distribution yields significant errors in the derived extinction [36], but the situation becomes even more complicated when considering the impact of having a bimodal distribution rather than a monomodal one. For background sulfate aerosols, a typical assumption for the analysis of limb scattering measurements is a monomodal distribution with r_m = 80 nm and S = 1.6. This assumes that the signal is dominated by the fine mode, a decision based on particle counter observations that the fine mode is significantly more plentiful than the coarse mode [28]. However, scattering efficiency increases dramatically with increasing size. Resonances in the Mie scattering also appear to be playing a role in the relative extinction for the two modes. Larger (coarse) particles have a resonant response at lower wavenumber than the smaller (fine) particles, which further enhances the extinction of coarse mode particles relative to fine mode particles in the near-infrared and visible regions. This is particularly evident for the very large particles from Tonga where the coarse mode resonance creates a distinct minimum in transmittance (see Fig. 5) but is also noticeable even at background levels (see Fig. 7). At wavelengths often used in aerosol studies, the scattering signal from the coarse mode will be comparable to or greater than that from the fine mode, despite the disparity in number densities.

An analysis approach developed for the Ozone Mapping and Profiler Suite Limb Profiler (OMPS-LP) uses a bimodal distribution with fixed parameters for fine and coarse modes, adjusting the fraction of coarse mode particles in the analysis [37]. The fixed parameters are based on measurements following the Pinatubo eruption [38], which created the largest perturbation in stratospheric sulfate aerosols in recent memory [1], opening the possibility that the values used are not representative of sulfates at background levels (e.g., may be too large).

Lidar studies could also be impacted by assuming a monomodal size distribution in the analysis rather than bimodal. A multiwavelength polarization Raman lidar study identified aerosols in the Arctic following the Raikoke eruption as smoke particles rather than sulfate aerosols [39]. The measurements were presumably too sensitive to fit satisfactorily with a monomodal sulfate model. Absorption at short wavelengths by Black Carbon in smoke particles (sulfate aerosols lack appreciable absorption in the visible region) would provide a means to empirically match the calculations to the observations, but the unexpected wavelength dependence presumably arose from a changing mix of contributions from the two modes as a function of wavelength (see Fig. 3b). The shape of the spectrum in the infrared (i.e., in the ACE-FTS region) definitively identifies aerosols in the Arctic following the Raikoke eruption as sulfate [11].

Similarly, an approach to identify aerosol type from a single derived parameter (slope of the SAGE III/ISS spectrum) inaccurately labeled some Raikoke sulfate aerosols as smoke particles [40]. The bimodal distribution generated by the Raikoke eruption likely deviated too much from the assumptions implicit in using a monomodal distribution for the approach to work as intended for this volcanic event.

Past sulfate aerosol studies of ACE-FTS measurements have assumed a distribution spread of 1.3 for the monomodal size distribution [11,16]. The results presented here indicate a value of 1.5 to 1.6 would be more representative. As mentioned previously, the shape of the infrared spectrum does not depend strongly on the assumed value of S. Extinction in the infrared comes primarily from absorption, for which the shape of the spectrum does not depend on the size of the particle. Composition (wt% H_2SO_4) and temperature determine the shape of the absorption spectrum. There is, however, a modest contribution from scattering in ACE-FTS measurements, smaller in magnitude than the absorption signal. The scattering contribution is strongest at higher wavenumbers (above ~3500 cm^{-1}) and appears to come mostly from the coarse mode for the examples in the current study. The spectral shape for this contribution depends on particle size but can be accurately reproduced with different combinations of S and median radius. In the analysis of ACE-FTS measurements by themselves (i.e., without SAGE data), fixing S to a different value makes a dramatic change in the fitted value for

median radius but generates only a subtle change in the value determined for wt% H_2SO_4.

Considering ACE-FTS data from sr86637 15.2 km (see Fig. 2), fixing S to 1.3 yields a median radius of 0.219 ± 0.005 μm and wt% H_2SO_4 = 73.3 ± 0.2 (errors are the random fitting errors and do not include systematic contributions). Fixing S to 1.55 yields a median radius of 0.127 ± 0.004 μm and wt% H_2SO_4 = 73.1 ± 0.2. The quality of the least squares fitting is nearly identical for the two different values of S (i.e., the fitting residuals are close to identical), which means assuming an incorrect value for this parameter has no bearing on determining whether the aerosols are sulfate rather than smoke [11]. All sulfate aerosols median radii reported in previous ACE-FTS studies [11,16] are significantly overestimated, although no scientific interpretation of median radius was performed in these studies. There could be a small systematic error introduced into previously determined values for wt% H_2SO_4 (where S = 1.3 was assumed) that should typically be well under 0.5 %.

With S(fine) fixed in the analysis presented here, care must be taken in the interpretation of N_0(fine)/N_0(coarse), but the results show a tendency for a lower ratio at lower altitudes, presumably a consequence of larger particles experiencing greater settling. The effect is especially pronounced in the Tonga results.

Many sulfate aerosol studies fix wt% H_2SO_4 to 75 %, as a matter of convenience. Results in Table 2 through 4 show that this is generally not accurate. In the lower stratosphere, wt% H_2SO_4 typically decreases with decreasing altitude, driven by decreasing temperatures and increasing H_2O concentration [16]. In atmospheric regions with a combination of relatively high H_2O levels and low temperature, H_2SO_4 in the droplet can drop below 50 % [11,16]. If H_2O concentration and temperature are known, an empirical function can be used to calculate a reasonably accurate estimate for wt% H_2SO_4 [16] rather than using a fixed value, in cases where the measurement set lacks the infrared aerosol spectrum from which the information can be accurately derived.

The bimodal distributions for the two volcanic eruptions observed in this study were very different. The coarse mode was significantly more enhanced for Tonga measurements than for Raikoke. The absorption signal (below ~3500 cm^{-1} in the ACE-FTS measurement) was dominated by the fine mode for background and Raikoke cases but was slightly larger for the coarse mode in Tonga measurements.

The relatively small number of extreme close coincidences between ACE and SAGE III/ISS limits the ability to explore volcanic eruptions more fully, i.e., to look at different eruptions or to distinguish different contributions to volcanic sulfate evolution (e.g., changing seasonal conditions versus aerosol aging). The ACE satellite has a Visible/Near IR instrument called MAESTRO (Measurement of Aerosol Extinction in the Stratosphere and Troposphere Retrieved by Occultation) [6] that shares the same line-of-sight as ACE-FTS, making every measurement a coincident one. Combining information from the two instruments would provide a powerful data set for a quantitative study of sulfate aerosols. Many volcanoes have been measured over the 19+ years of ACE observations collected to date. Information from the 1 μm imager on the ACE satellite can also be combined with ACE-FTS data using the same approach as was used to splice in SAGE III/ISS data, although the resulting wavenumber coverage would be insufficient to accurately derive bimodal size distribution parameters.

The preliminary results presented here indicate great promise for the combination of ACE-FTS and Visible/Near IR measurements, but some questions remain. For background sulfates, both S(fine) and S(coarse) were fixed in the least squares analysis to avoid excessive random errors, which appeared to be related to systematic residuals of unknown origin in the SAGE data. The residuals were small, but when pushing the limits of the information content by fitting for a bimodal size distribution, even small systematic effects can have a major impact. Identifying the source (s) of the systematic fitting residuals in the SAGE data is required to reliably investigate bimodal size distribution for background sulfates and could also change the results obtained for volcanically enhanced

sulfates.

Values obtained for N_o(fine)/N_o(coarse) were generally smaller than expected from particle counter observations [28]. The extinction measurements analyzed here were more sensitive to larger particles, as evinced by the need to fix S(fine) for the volcanic measurements, and it is possible this leads to an undercounting of the fine mode, if a subset of very fine particles is seen by particle counters but provides little contribution to the measured extinction. There is also a question of whether assuming a pseudo gas cell measurement (rather than determining altitude profiles for the fitted quantities) has an impact on the results.

Data availability

ACE-FTS data can be accessed at the following web portal: https://databace.scisat.ca/level2/ace_v4.1_v4.2/display_data.php. First time data users can register at https://database.scisat.ca/l2signup.php. SAGE III/ ISS data are available from NASA's Atmospheric Science Data Center (https://eosweb.larc.nasa.gov/). Data from Figs. 2, 4, and 6, not available elsewhere, are provided as supplementary information to this article.

Declaration of Competing Interest

The authors declare that they have no known competing financial interests or personal relationships that could have appeared to influence the work reported in this paper.

Supplementary materials

Supplementary material associated with this article can be found, in the online version, at doi:10.1016/j.jqsrt.2023.108815.

Appendix

Table A

Table A

Alternative bimodal distribution results for measurements associated with the Raikoke eruption, with nearly identical fitting quality to the results in Table 2 but a different nature for the coarse mode. The bimodal results in Table 2 are deemed the preferred solution.

ACE event	Altitude (km)	Fine r_m (μm)	Fine S	Coarse r_m (μm)	Coarse S	N_o(fine)/ N_o(coarse)
sr86637	17.5	0.056	1.65*	0.39	1.30	420
	15.2	0.059	1.65*	0.44	1.15	380
	13.0	0.073	1.65*	0.48	1.13	320
	10.9	0.075	1.65*	0.49	1.19	360
sr88283	17.0	0.063	1.65*	0.43	1.14	450
	16.0	0.069	1.65*	0.44	1.12	350
	15.1	0.065	1.65*	0.43	1.12	340
	14.1	0.063	1.65*	0.43	1.12	330
	13.2	0.059	1.65*	0.41	1.12	270
	12.3	0.060	1.65*	0.42	1.12	350
	11.6	0.061	1.65*	0.43	1.11	350
	10.8	0.068	1.65*	0.46	1.11	320
ss89663	16.6	0.061	1.65*	0.42	1.12	560
	14.5	0.061	1.65*	0.41	1.12	400
	12.6	0.067	1.65*	0.43	1.12	370
	11.1	0.067	1.65*	0.44	1.12	400

* S fixed to the indicated value in the analysis.

References

[1] Kremser S, Thomason LW, von Hobe M, Hermann M, Deshler T, Timmreck C, et al. Stratospheric aerosol - observations, processes, and impact on climate. Rev Geophys 2016;54:278–335. https://doi.org/10.1002/2015RG000511.

[2] Gleason JF, Bhartia PK, Herman JR, McPeters R, Newman P, Stolarski RS, et al. Record low global ozone in 1992. Science 1993;260:523–6. https://doi.org/10.1126/science.260.5107.523.

[3] Rasch PJ, Crutzen PJ, Coleman DB. Exploring the geoengineering of climate using stratospheric sulfate aerosols: the role of particle size. Geophys Res Lett 2008;35: L02809. https://doi.org/10.1029/2007GL032179.

[4] Robock A. Volcanic eruptions and climate. Rev Geophys 2000;38:191–219. https://doi.org/10.1029/150GM11.

[5] Persad GG, Samset BH, Wilcox LJ. Aerosols must be part of climate risk assessments. Nature 2022;611:662–4. https://doi.org/10.1038/d41586-022-03763-9.

[6] Bernath PF. The Atmospheric Chemistry Experiment (ACE). J Quant Spectrosc Radiat Transf 2016;186:3–16. https://doi.org/10.1016/j.jqsrt.2016.04.006.

[7] Buijs HL, Soucy MA, Lachance RL. ACE-FTS hardware and level 1 processing. The atmospheric chemistry experiment ace at 10: a solar occultation anthology. Hampton, VA, USA: Deepak Publishing; 2013. p. 53–80. a.

[8] Boone CD, Bernath PF, Lecours M. Version 5 retrievals for ACE-FTS and ACE-imagers. J Quant Spectrosc Radiat Transf 2023;310:108749. https://doi.org/10.1016/j.jqsrt.2023.108749.

[9] Wrana F, von Savigny C, Zalach J, Thomason LW. Retrieval of stratospheric aerosol size distribution parameters using satellite solar occultation measurements at three wavelengths. Atmos Meas Tech 2021;14:2345–57. https://doi.org/10.5194/amt-14-2345-2021.

[10] Muser LO, Hoshyaripour GA, Bruckert J, Horváth Á, Malinina E, Wallis S, et al. Particle aging and aerosol–radiation interaction affect volcanic plume dispersion: evidence from the Raikoke 2019 eruption. Atmos Chem Phys 2020;20:15015–36. https://doi.org/10.5194/acp-20-15015-2020.

[11] Boone CD, Bernath PF, LaBelle K, Crouse J. Stratospheric aerosol composition observed by the atmospheric chemistry experiment following the 2019 Raikoke eruption. J Geophys Res 2022;127:e2022JD036600. https://doi.org/10.1029/2022JD036600.

[12] Kloss C, Berthet G, Sellitto P, Ploeger F, Taha G, Tidiga M, et al. Stratospheric aerosol layer perturbation caused by the 2019 Raikoke and Ulawun eruptions and

their radiative forcing. Atmos Chem Phys 2021;21:535–60. https://doi.org/10.5194/acp-21-535-2021.

[13] Matoza RS, Fee D, Assink JD, Iezzi AM, Green DN, Kim K, et al. Atmospheric waves and global seismoacoustic observations of the January 2022 Hunga eruption, Tonga. Science 2022;377:95–100. https://doi.org/10.1126/science.abo7063.

[14] Proud SR, Prata A, Schmauss S. The January 2022 eruption of Hunga Tonga-Hunga Ha'apai volcano reached the mesosphere. Science 2022;378:554–7. https://doi.org/10.1126/science.abo7063.

[15] Zhu Y, Bardeen CG, Tilmes S, Mills MJ, Wang X, Harvey VL, et al. Perturbations in stratospheric aerosol evolution due to the water-rich plume of the 2022 Hunga-Tonga eruption. Commun Earth Environ 2022;3:248. https://doi.org/10.1038/s43247-022-00580-w.

[16] Bernath PF, Boone C, Pastorek A, Cameron D, Lecours M. Satellite characterization of global stratospheric sulfate aerosols released by Tonga volcano. J Quant Spectrosc Radiat Transf 2023;299:108520. https://doi.org/10.1016/j.jqsrt.2023.108520.

[17] Heathfield AE, Newnham DA, Ballard J, Grainger RG, Lambert A. Infrared and visible Fourier-transform spectra of sulfuric-acid–water aerosols at 230 and 294K. Appl Opt 1999;38:6408–20. https://doi.org/10.1364/AO.38.006408.

[18] Boone CD, Bernath PF, Cok D, Jones SC, Steffen J. Version 4 retrievals for the Atmospheric Chemistry Experiment Fourier Transform Spectrometer (ACE-FTS) and imagers. J Quant Spectrosc Radiat Transf 2020;247:106939. https://doi.org/10.1016/j.jqsrt.2020.106939.

[19] Gordon IE, Rothman LS, Hill C, Kochanov RV, Tan Y, Bernath PF, et al. The HITRAN 2016 molecular spectroscopic database. J Quant Spectrosc Radiat Transf 2017;203:3–69. https://doi.org/10.1016/j.jqsrt.2017.06.038.

[20] Boone CD, Bernath PF. Tangent height determination from the N_2 continuum for the Atmospheric Chemistry Experiment Fourier Transform Spectrometer. J Quant Spectrosc Radiat Transf 2019;238:106481. https://doi.org/10.1016/j.jqsrt.2019.04.033.

[21] Thibault F, Menoux V, Le Doucen R, Rosenmann L, Hartmann JM, Boulet C. Infrared collision-induced absorption by O_2 near 6.4μm for atmospheric applications: measurements and empirical modeling. Appl Opt 1997;36(3):563–7. https://doi.org/10.1364/AO.36.000563.

[22] Cousin C, Doucen RL, Boulet C, Henry A. Temperature dependence of the absorption in the region beyond the 4.3-μm band head of CO_2 2: N_2 and O_2 broadening. Appl Opt 1985;24(22):3899–907. https://doi.org/10.1364/AO.24.003899.

[23] Lund Myhre CE, Christensen DH, Nicolaisen FM, Nielsen CJ. Spectroscopic study of aqueous H_2SO_4 at different temperatures and compositions: variations in dissociation and optical properties. J Phys Chem A 2003;107:1979–91. https://doi.org/10.1021/jp026576n.

[24] Wrana F, von Savigny C, Zalach J, Thomason LW. Retrieval of stratospheric aerosol size distribution parameters using satellite solar occultation measurements at three wavelengths. Atmos Meas Tech 2021;14:2345–57. https://doi.org/10.5194/amt-14-2345-2021.

[25] Palmer KF, Williams D. Optical constants of sulfuric acid; application to the clouds of venus? Appl Opt 1975;14:208–19. https://doi.org/10.1364/AO.14.000208.

[26] Steele HM, Hamill P. Effects of temperature and humidity on the growth and optical properties of sulphuric acid-water droplets in the stratosphere. J Aerosol Sci 1981;12:517–28. https://doi.org/10.1016/0021-8502(81)90054-9.

[27] Pueschel RF, Russell PB, Allen DA, Ferry GV, Snetsinger KG, Livingston JM, Verma S. Physical and optical properties of the Pinatubo volcanic aerosol: aircraft observations with impactors and a Sun-tracking photometer. J Geophys Res 1994;99(D6):12915–22. https://doi.org/10.1029/94JD00621.

[28] Deshler T, Luo B, Kovilakam M, Peter T, Kalnajs LE. Retrieval of aerosol size distributions from *in situ* particle counter measurements: instrument counting efficiency and comparisons with satellite measurements. J Geophys Res Atmos 2019;24:5058–87. https://doi.org/10.1029/2018JD029558.

[29] Murphy DM, Froyd KD, Bourgeois I, Brock CA, Kupc A, Peischl J, et al. Radiative and chemical implications of the size and composition of aerosol particles in the existing or modified global stratosphere. Atmos Chem Phys 2021;21:8915–32. https://doi.org/10.5194/acp-21-8915-2021.

[30] Hansen JE, Travis LD. Light scattering in planetary atmospheres. Space Sci Rev 1974;16:527–610. https://doi.org/10.1007/BF00168069.

[31] Wrana F, Niemeier U, Thomason LW, Wallis S, von Savigny C. Stratospheric aerosol size reduction after volcanic eruptions. Atmos Chem Phys 2023;23:9725–43. https://doi.org/10.5194/acp-23-9725-2023.

[32] Khaykin S, Podglajen A, Ploeger F, Grooss JU, Tence F, Bekki S, et al. Global perturbation of stratospheric water and aerosol burden by Hunga eruption. Commun Earth Environ 2022;3:316. https://doi.org/10.1038/s43247-022-00652-x.

[33] von Savigny C, Hoffmann CG. Issues related to the retrieval of stratospheric-aerosol particle size information based on optical measurements. Atmos Meas Tech 2020;13:1909–20. https://doi.org/10.5194/amt-13-1909-2020.

[34] Madhavan BL, Kudo R, Ratnam MV, Kloss C, Berthet G, Sellitto P. Stratospheric aerosol characteristics from the 2017–2019 volcanic eruptions using the SAGE III/ISS observations. Remote Sens 2023;15:29. https://doi.org/10.3390/rs15010029.

[35] Bourassa AE, Rieger LA, Lloyd ND, Degenstein DA. Odin-OSIRIS stratospheric aerosol data product and SAGE III intercomparison. Atmos Chem Phys 2012;12:605–14. https://doi.org/10.5194/acp-12-605-2012.

[36] Bourassa AE, Zawada DJ, Rieger LA, Warnock TW, Toohey M, Degenstein DA. Tomographic retrievals of Hunga Tonga-Hunga Ha'apai volcanic aerosol. Geophys Res Lett 2023;50:e2022GL101978. https://doi.org/10.1029/2022GL101978.

[37] Loughman R, Bhartia PK, Chen Z, Xu P, Nyaku E, Taha G. The Ozone Mapping and Profiler Suite (OMPS) Limb Profiler (LP) Version 1 aerosol extinction retrieval algorithm: theoretical basis. Atmos Meas Tech 2018;11:2633–51. https://doi.org/10.5194/amt-11-2633-2018.

[38] Pueschel RF, Russell PB, Allen DA, Ferry GV, Snetsinger KG, Livingston JM, Verma S. Physical and optical properties of the Pinatubo volcanic aerosol: aircraft observations with impactors and a Sun-tracking photometer. J Geophys Res 1994;99:12915–22. https://doi.org/10.1029/94JD00621.

[39] Ohneiser K, Ansmann A, Chudnovsky A, Engelmann R, Ritter C, Veselovskii I, et al. The unexpected smoke layer in the high arctic winter stratosphere during MOSAiC 2019–2020. Atmos Chem Phys 2021;21:15783–808. https://doi.org/10.5194/acp-21-15783-2021.

[40] Knepp TN, Thomason L, Kovilakam M, Tackett J, Kar J, Damadeo R, Flittner D. Identification of smoke and sulfuric acid aerosol in SAGE III/ISS extinction spectra. Atmos Meas Tech 2022;15:5235–60. https://doi.org/10.5194/amt-15-5235-2022.